PCCP

Accepted Manuscript

ROYAL SOCIETY OF CHEMISTRY

www.rsc.org/pccp

A Molecular Theory for Optimal Blue Energy Extraction by Electrical Double Layer Expansion

Xian Kong[1,2], Alejandro Gallegos[1], Diannan Lu[2], Zheng Liu[2*] and Jianzhong Wu[1*]*

[1] Department of Chemical and Environmental Engineering and Department of Mathematics, University of California, Riverside, CA 92521, USA

[2] Department of Chemical Engineering, Tsinghua University, Beijing 100084, China

ABSTRACT

Electrical double layer expansion (CDLE) has been proposed as a promising alternative to reverse electrodialysis (RED) and pressure retarded osmosis (PRO) processes for extracting osmotic power generated by the salinity difference between freshwater and seawater. The performance of the CDLE process is sensitive to the configuration of porous electrodes and operation parameters for ion extraction and release cycles. In this work, we use a classical density functional theory (CDFT) to examine how the electrode pore size and charging/discharging potentials influence the thermodynamic efficiency of the CDLE cycle. The existence of an optimal charging potential that maximizes the energy output for a given pore configuration is predicted, which varies substantially with the pore size, especially when it is smaller than 2 nm. The thermodynamic efficiency is maximized when the electrode has a pore size about twice the ion diameter.

Introduction

The entrance of fresh river water to the oceans induces energy dissipation on the order of 2 kJ/L owing to the free energy of mixing for electrolytes of different concentrations[1]. The so-called osmotic power or "Blue Energy" can be harvested with various processes to convert the chemical energy into mechanical or electrical work. Because of the vast volume of river water discharging into the oceans globally, blue energy is attractive for its potential in providing a clean, self-replenishing avenue for renewable power generation with minimal carbon footprint and pollutions.

Among a number of procedures to utilize the blue energy[2], "capacitive mixing" (CAPMIX) represents a relatively new technique but it emerges fast in part due to rapid developments in electric double layer supercapacitors and porous electrodes with ultra-large specific surface areas[3, 4]. By cyclic charging and discharging in seawater and freshwater respectively, nanoporous electrodes are able to adsorb and desorb a large amount of ionic species. The controlled ion transfer from seawater to fresh river water amounts to a reverse deionization process with a net output of the electrical energy. Specifically, CAPMIX includes three major techniques, *i.e.*, "Capacitive Double Layer Expansion" (CDLE)[5], "Capacitive Donnan Potential" (CDP)[6], and "Mixing Entropy Battery" (MEB)[7]. The reverse operations of these CAPMIX methods correspond to "Capacitive Deionization"[8], "Membrane Capacitive Deionization"[9], and "Desalination Battery"[10], respectively.

CDLE is the original CAPMIX technique first proposed by Brogioli[5]. It does not involve an ion-selective membrane as in CDP, and is free of chemical reactions as occurring in MEB. As a result, the CDLE technique has no issues related to membrane fouling or rate limiting by slow chemical reactions, making it more sustainable and efficient than other CAPMIX processes.

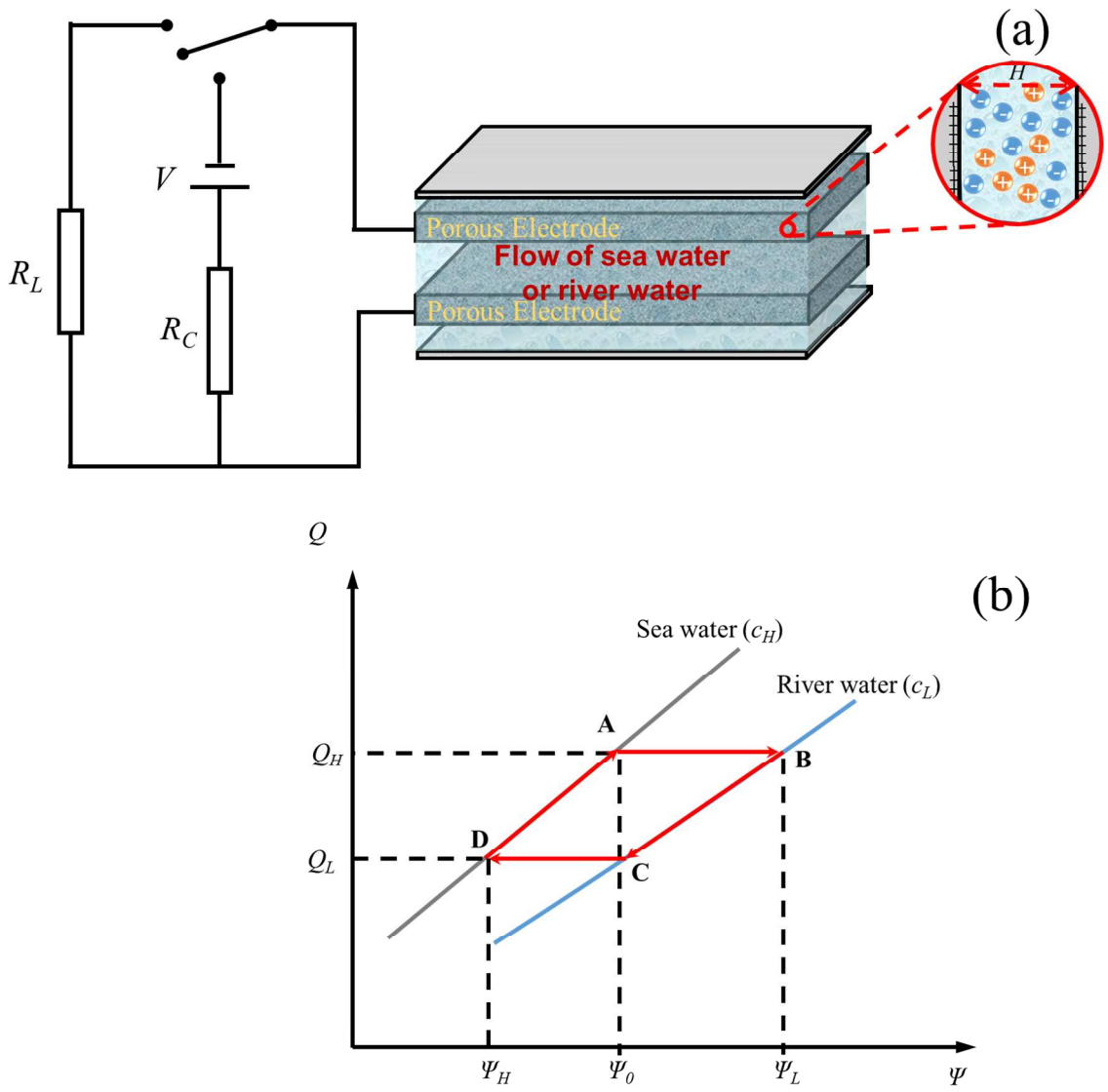

Figure 1. (a) A schematic setup for Capacitive Double Layer Expansion (CDLE) processes. The device consists of an external circuit for charging (power V and capacitance resistance R_C) and discharging (load R_L) and two porous electrodes in alternative contacts with fresh and seawater. (b) The thermodynamic cycle in terms of variations of the electrode charge and the potential of the cathode, *i.e.*, the Q-Ψ curves. As explained in the text, points A, B, C, D in this plot represent four thermodynamic states of the cathode, c_H and c_L are electrolyte concentrations of seawater and river water, respectively.

Figure 1(a) presents a schematic setup for a typical CDLE process. It consists of an external circuit for charging and discharging of a pair of porous electrodes that are submerged alternately in seawater and river water, respectively. Because the energy required for the

electrode charging in seawater is smaller than the energy output from discharging of the same electrode in river water, the cyclic process yields a net energy output corresponding to the conversion of the osmotic power to electrical energy. Figure 1(b) shows the thermodynamic cycle for the blue energy extraction process in terms of the variations of the surface charge and the electrical potential of the porous electrode (here cathode). The operation consists of four reversible processes. First, the electrode is immersed in seawater with charging potential Ψ_0 imposed by the external circuit. The equilibrium charge of the electrode Q_H is determined by the charging potential Ψ_0 and the electrolyte concentration of seawater c_H. During the reversible process from state A to B, the electrode is disconnected from the external circuit while the surrounding fluid is shuffled from seawater to river water. The decrease in ion concentration in the bulk raises the electrode potential from Ψ_0 to Ψ_L without changing the electrode charge. At state B, the electrical potential Ψ_L is determined by the electrode charge density Q_H and the electrolyte concentration of river water c_L. Next, the electrode is connected to an electrical load (R_L in Fig.1a), leading to the reduction of both the electrical potential and the surface charge. The electrical potential at state C defines the discharging potential, Ψ_0', which is usually set to be the same as the charging potential, namely, $\Psi_0' = \Psi_0$. During the reversible process from state B to C, the electrode remains in contact with river water so that the bulk electrolyte concentration is constant. As a result, the charge density at state C (Q_L) is solely determined by the discharging potential. During the third step from state C to D, river water is replaced with seawater while the electrodes are again disconnected from the external circuit. A raise in ion concentration further decreases the electrode potential from Ψ_0 to Ψ_H without changing the electrode charge density (Q_L). Finally, the thermodynamic cycle is closed after raising the electrode potential from Ψ_H (state D) to Ψ_0 (state A). The energy input for electrode charging depends on the final potential

Ψ_0 and the seawater electrolyte concentration c_H. Because the charging and discharging energies are directly related to the electrode charge and electrical potential, the enclosed area ABCD in Fig.1(b) represents the net energy that can be extracted from the thermodynamic cycle[11].

The net energy output is sensitive to the microscopic structure of the porous electrodes and the operation parameters in ion extraction and release cycles[12]. To optimize the CDLE process, we need to analyze the maximum energy extracted or, alternatively, the maximum energy extraction efficiency as a function of the operation parameter (Ψ_0). Toward that end, an accurate theoretical model is required to predict the charge-potential curves in the thermodynamic cycle. While the charge-potential relationship has been well established for electrical double layers (EDLs) near a flat surface, the situation is much more complicated for electrodes with nanopores comparable to the ionic size[13, 14]. In that case, ion excluded volume effects, which is often ignored in conventional EDL theories, becomes significant and may dominate the charging behavior. Nanoporous electrodes have been used extensively in recent developments of supercapacitors and are promising for applications to CAPMIX processes. Because the capacitance of the electrodes is directly correlated with the surface area of micropores, we expect that the performance of the CDLE process can be drastically improved by using nanostructured electrodes with ultra-high specific surface area and micropores with the pore size comparable to the ion diameters[15-18].

Conventional methods like the Gouy-Chapman-Stern (GCS) theory[19, 20] is adequate to describe the charging behaviors of EDLs in macroscopic pores[13] at relatively low surface electric potential[21]. The mean-field method breaks down for electrodes with small pores because it ignores electrostatic correlations and the ionic excluded volume effects[21, 22]. Boon *et al.* proposed a classical density functional theory (CDFT) based on the mean-field electrostatics and

a lattice-gas model for ionic steric repulsions[23]. The lattice-gas model was able to capture certain features of the ionic size effects but ignores electrostatic correlations. Recently, Härtel *et al*. compared CDFT with different modifications of the Poisson-Boltzmann theory[24]. They emphasized the importance of size and ion correlation effects for a faithful description of electrolyte solutions in micropores. In this work, we report an alternative CDFT that provides a more faithful depiction of ionic distributions under nanoscale confinement and subsequently, the Q-Ψ curves for the CDLE cycle. By comparing theoretical results from the CDFT and GCS models, we provide new insights into how the performance of CDLE processes is influenced by ionic size and electrostatic correlations. The new theoretical framework can be utilized to predict optimal electrode parameters and charging potential to maximize blue energy extraction.

Molecular Models and Methods

Electrode and electrolyte models

To minimize the number of system and operation parameters to describe the CDLE cycle, we assume that the charging/discharging parameters at the positive and negative electrodes are identical other than the opposite signs. The positive-negative symmetry implies that cations and anions have the same size and electrostatic valence value and that the cathodes and anodes have the same porous structure. For simplicity, each electrode pore is described as a slit of width H (Fig. 1a) with perfectly smooth surfaces as represented by a hard-wall potential. At any moment, the two surfaces of the slit pore have the same electric potential Ψ.

Approximately, seawater and river water can be represented by aqueous solutions of NaCl with different concentrations. The thermodynamic properties of simple electrolytes can be described quantitatively with a so-called restrictive primitive model where cations and anions are

depicted as monovalent ($Z_+=-Z_-=1$) charged hard spheres of the same diameter ($\sigma_+ = \sigma_- = 0.5$ nm), and the solvent (*i.e.* water) is a dielectric continuum ($\varepsilon_r = 78.4$).

The Q-Ψ curves

We used the classical density functional theory (CDFT) to calculate the ion density profiles in the direction perpendicular to the surface of each nanochannel (*viz*., z-direction)[25]. According to CDFT, the density of i^{th} ion at position z is given by

$$\rho_i(z) = \rho_i^{bulk} \exp\left[-\beta V_i(z) - \beta Z_i e\varphi(z) - \beta\Delta\mu_i^{ex}(z)\right] \tag{1}$$

where z is the vertical distance from one surface of the slit pore, ρ_i^{bulk} denotes the bulk concentration of ion i, $\varphi(z)$ represents the local electrostatic potential, e is unit charge, $\beta = 1/(k_B T)$ with k_B being the Boltzmann constant and T being the absolute temperature, and $\Delta\mu_i^{ex}(z)$ stands for the deviation of the local excess chemical potential for ion i from that in the bulk. In Eq.(1), external potential $V_i(z)$ accounts for the non-electrostatic component of the ion-wall interaction

$$V_i(z) = \begin{cases} \infty, & z \geq H - \dfrac{\sigma_i}{2} \ \ or \ \ z \leq \dfrac{\sigma_i}{2} \\ 0, & \dfrac{\sigma_i}{2} < z < H - \dfrac{\sigma_i}{2} \end{cases} \tag{2}.$$

The local electrostatic potential $\varphi(z)$ and the ionic density profiles $\rho_i(z)$ are related according to the Poisson equation

$$\frac{d^2\varphi(z)}{dz^2} = -\frac{\rho_e(z)}{\varepsilon_0\varepsilon_r} \tag{3}$$

where $\rho_e(z) = \sum_{i=\pm} Z_i e \rho_i(z)$ represents the local charge density, ε_0 is the vacuum permittivity (8.854×10^{-12} F·m^{-1}), ε_r is relative permittivity of water (78.4 at 25 ^{o}C). From Eqs.(1-3), we can solve for the local ionic densities and the local electrostatic potential with the boundary conditions $\varphi(0) = \varphi(H) = \Psi$. The precise form of the excess chemical potential for each ion and numerical details for solving these equations are provided in Supporting Information. If we neglect contributions to the local excess chemical potential due to ionic excluded volume effects and electrostatic correlations, Eqs.(1-3) reduce to those given by the conventional Poisson-Boltzmann theory for describing inhomogeneous ionic distributions. In essence, CDFT provides a systematic way to calculate the thermodynamic non-ideality due to intermolecular interactions[25-27]. The detail DFT equations and their calibrations have been reported before[25-27]. Supporting Information recapitulates only the relevant equations used in this work.

From the ionic density profiles, we can calculate the surface charge density on each of the two electrode surfaces according to the macroscopic electrostatic neutrality condition for the entire pore

$$Q = -\frac{1}{2}\int_0^H [\sum_i Z_i e \rho_i(z)] dz \,. \tag{4}$$

The Q-Ψ curves are obtained by repeating the DFT calculations for different cathode potentials.

Extracted electric energy per cycle

As illustrated in Fig. 1(b), we can obtain the net electrical energy extracted per cycle based on the Q-Ψ curves at two different ion concentrations that correspond to those of seawater and river water. For a given charging potential Ψ_0, the intersections of $\Psi = \Psi_0$ with the two Q-Ψ curves determine states A and C in Fig.(1b), and the horizontal lines passing through A and C

defines states B and D on the *Q*-Ψ curves, respectively. The network extracted pre cycle, *W*, is obtained by numerical integration for the area enclosed by ABCDA.

The thermodynamic efficiency η of the CDLE cycle is defined by net energy output (*W*) divided by the change in the Gibbs free energy when N_s moles of salt ions are transferred from seawater to river water

$$\eta = \frac{W}{\Delta N_s(\mu_H - \mu_L)} \tag{5}$$

In Eq.(5), μ_H and μ_L are the mean ionic chemical potentials in seawater and river water, respectively; ΔN_s corresponds to the difference between the number of ions in states A and C in Fig. 1b. Since state A and C represent states of the solution in the electrode pore that are in equilibrium with sea water and salt water, they represent the state which have the most and least ions in the electrode pore. The mean ionic chemical potential is defined by the ion concentration as explained in Supporting Information. In this work, we assume that the NaCl concentration in river water is 20 mM and that of the seawater is 500 mM. The corresponding reduced mean ionic chemical potentials are $\beta\mu_H$ = -2.940, and $\beta\mu_L$ =-6.486, respectively.

Results and Discussions

Q-Ψ curves

The *Q*-Ψ curves are needed to predict the net electrical energy that can be extracted from each thermodynamic cycle of the CDLE process. In Figure 2, we compare two *Q*-Ψ curves predicted by CDFT with experimental data for a planar electrode in contact with aqueous electrolytes at representative salt concentrations. Also shown in this figure are predictions from the Gouy-Chapman-Stern (GCS) theory, a conventional method to describe the charging behavior of electric double layers and was used in an earlier publication[28]. To convert the

experimental results for the charge density in terms of C/g to C/m^2, we adopt a specific surface area of the porous electrode (900m^2/g) in both CDFT and GCS calculations[28]. This surface area is much smaller than the BET area of the material used in experiments (□1330 m^2/g). The experimental data should be rescaled (linearly) if a different specific area is used.

For electrolytes with monovalent ion pairs, the GCS theory gives an analytical relation between the surface charge density and the surface charge potential[21, 29],

$$\Psi = \frac{2k_BT}{e}\sinh^{-1}\left(\frac{Q}{\sqrt{8C_sN_A\varepsilon_0\varepsilon_rk_BT}}\right) + \frac{l_sQ}{\varepsilon_0} \tag{6}$$

where the first term on the right side accounts for the contribution from the EDL layer or diffusive layer, and the second term results from the Stern layer. In the GCS model, the thickness of the Stern layer l_s is treated as a fitting parameter[30].

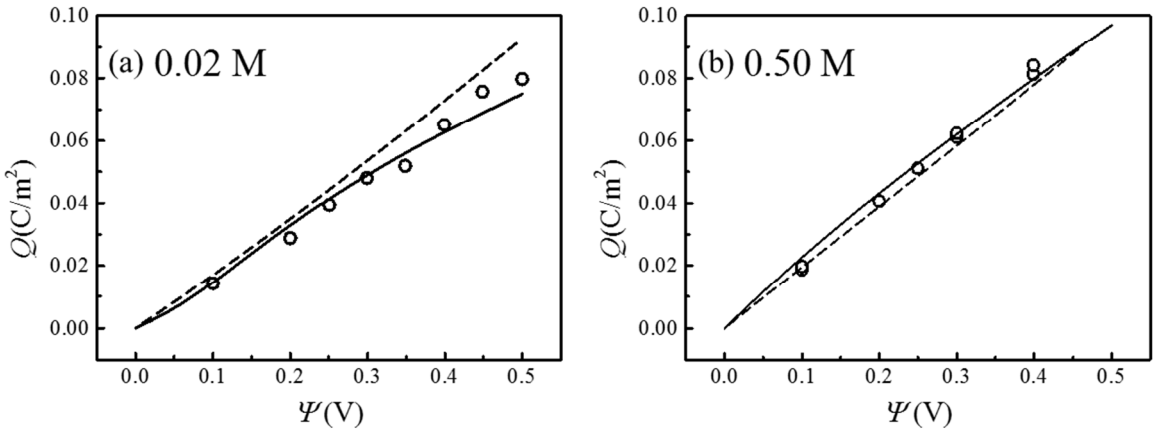

Figure 2. The charge density (Q) *vs.* electric potential (Ψ) for a planar electrode in contact with river water ([NaCl]= 20 mM) (a) and with seawater ([NaCl]= 500 mM) (b). The symbols are from experiments[30] (circles), the dashed lines are the predictions of the GCS theory[28], and the solid lines are the DFT predictions. The experimental data for the charge densities are obtained by converting the units from charge per gram (C/g) to charge per surface area (C/m^2). Both the specific area for the porous electrode (900m^2/g) and the Stern layer thickness (0.089 nm) are from the literature[30].

Figure 2 shows that both GCS and DFT give satisfactory Q-Ψ curves at low electric potentials. At high salt concentration, both theories reproduce the experimental results well for the range of electric potential studied in this work. The deviation between the two methods is most significant at large surface potential but low salt concentration (Fig. 2). In that case, GCS shows noticeable positive deviation from the experimental data while CDFT performs more satisfactory even though the latter entails no adjustable parameter. We expect that the GCS performance will further deteriorate for porous electrodes due to the large Debye length at low ion concentration. Besides, the ion size and correlation effects become more significant when the EDL expands throughout the electrode pore. Such effects can be accurately described by CDFT.

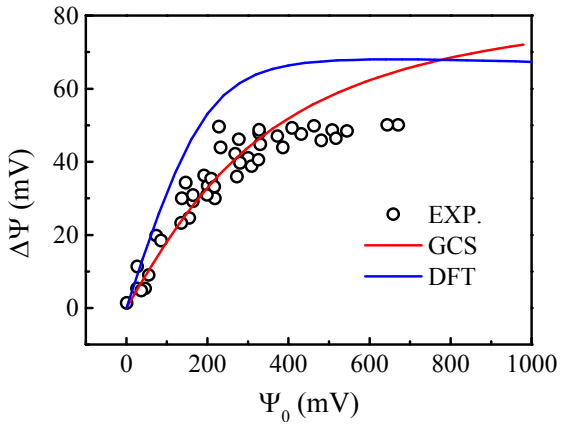

Figure 3. Potential rise ($\Delta\Psi$) of the electrode from state A to state B in Fig. 1 (b) obtained from experiments[31], GCS, and CDFT.

A key index to measure the performance of CDLE cycle is provided by the electrode potential rise ($\Delta\Psi$) when switching the electrolyte solution from seawater to river water in an open circuit[21]. Figure 3 compares $\Delta\Psi$ as a function of the charging potential Ψ_0 obtained from experiments, GCS and CDFT. We see that the GCS model agrees well the experimental data when the surface potential is lower than 200mV. However, it predicts a monotonic increase of the potential rise at larger surface potential, while the experimental data show a plateau. The

asymptotic behavior is well reproduced by CDFT. Nevertheless, Figure 3 shows noticeable discrepancy between CDFT and experiments, probably due to systematic errors in pore characterization. It is worth noting that Härtel *et al*. obtained a similar profile for $\Delta\Psi$ versus the charging potential for an electrode with pore width at 8 nm[24]. The plateau value (~100 mV) predicted in that work is higher than that shown in Figure 3 because of the differences in theoretical details and the model parameters (e.g., ion diameter in that work is 0.34 nm but here 0.5 nm).

Energy extracted per cycle

As discussed above, an integration of the Q-Ψ curves in the CDLE processes yields the net extractable energy per thermodynamic cycle. Figures 4(a) and 4(b) show the theoretical predictions , from DFT and GCS, respectively, of the extracted energy as a function of the charging potential and the electrode pore size. For electrodes with large pores, the GCS and CDFT predictions are similar at a small charging potential. At high charging potentials, however, the trend predicted by CDFT is quite different from that by GCS, in particular for electrodes with small pores. While the GCS model predicts a monotonic increase of the extracted work against the charging potential, the extracted work predicted by CDFT shows a maximum at an intermediate charging potential regardless of the pore size. The different trends may be attributed to the saturation effect at the electrode surface due to the ionic excluded volume, which is also responsible for the maximum extracted work per cycle at an intermediate charging potential. A similar non-monotonic behavior has been predicted by Jiménez *et. al.* using a modified Poisson-Boltzmann (MPB) theory that accounts for the ionic size effects[32]. According to the DFT predictions, the optimal charging potential is in the range of 100 mV to 230 mV, which is similar to that predicted by Jiménez *et. al.*[32]. In addition to thermodynamic conditions such as

temperature and electrolyte concentrations, we find that the optimal charging potential depends also on the electrode configuration, especially when the pore size is smaller than 2 nm. Because the charging potential is an operation parameter while the electrode pore size is materials property, the best performance of the EDLC cycle requires a careful tuning of these parameters.

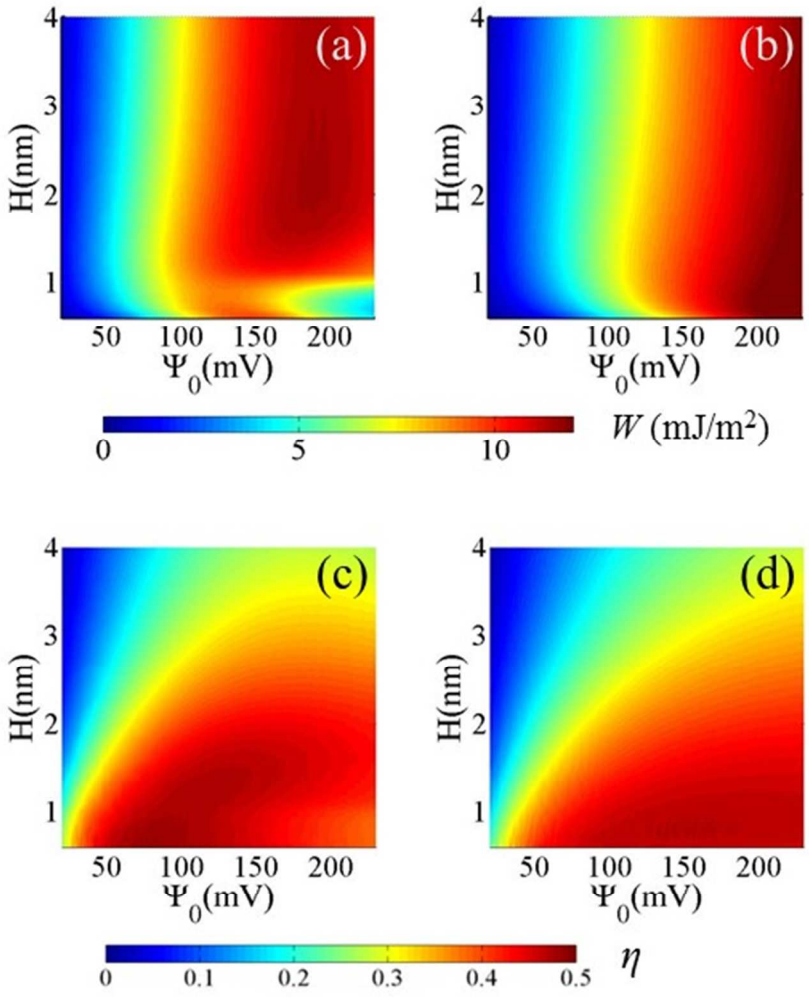

Figure 4. The effects of charging potential and electrode pore size on the net energy output (W) and the thermodynamic efficiency (η) of a CDLE process predicted by DFT(a and c) and by GCS (b and d).

Figures 4(c) and 4(d) show the theoretical predictions for the thermodynamic efficiency of the EDLC cycle as a function of the charging potential and the electrode pore size. It is evident that, for electrodes with large pores, CDFT and GCS yield similar results at low charging

potentials. For electrodes with small pores (< 2nm), however, the predictions from CDFT and GCS are very different and the discrepancy becomes more noticeable as the charging potential increases. While GCS predicts a monotonic rise of the thermodynamic efficiency as the charging potential is increased, a maximum thermodynamic efficiency is predicted according to the DFT calculations. Interestingly, both GCS and DFT predict that the thermodynamic efficiency decreases with the electrode pore size, favoring the use of nanostructured porous electrodes in the CDLE applications.

Optimal charging potential

We may define the optimal charging potential in terms of either the maximum work output Ψ_{0W}^{*} or the maximum thermodynamic efficiency $\Psi_{0\eta}^{*}$. As discussed above, in both cases the optimal charging potential is sensitive to the pore size.

Figure 5(a) shows variations of the optimal charging potentials versus the electrode pore size according to CDFT predictions. When the pore size is below 2 nm, the optimal charging potential for the net energy output is substantially higher than that for the thermodynamic efficiency. For pore sizes larger than 2 nm, however, these two potentials (Ψ_{0W}^{*} and $\Psi_{0\eta}^{*}$) are similar. For electrodes with small pores, both Ψ_{0W}^{*} and $\Psi_{0\eta}^{*}$ show a minimum when the pore size is about 1 nm, about twice of the ion diameter. In that case, each pore accommodates two single layers of counterions, leading to a maximum work output and thermodynamic efficiency.

Figure 5(b) presents the CDFT predictions for the maximum net energy output per surface area (*i.e.,* the energy density) and the maximum thermodynamic efficiency for the entire CDLE cycle. The energy density exhibits a minimum at a small pore size due to the non-monotonic variation of the optimal charging potential (see Figure 5a); the maximal energy density is reached when the pore size is about 2 nm and barely changes if the pore size is further

increased. While the energy density shows a minimum when the pore size is about 1 nm, the thermodynamic efficiency is the highest at this condition. In contrast, the thermodynamic efficiency is almost a constant for small pores but declines rapidly when the pore size is above 2 nm. As the pore size is changed from 1 nm to 4 nm, the thermodynamic efficiency falls from 0.45 to 0.25. Because both energy density and thermodynamic efficiency are important for practical applications, Figure 5(b) suggests that blue energy extraction by CDLE processes can be optimized by choosing an electrode with an appropriate pore size that matches the charging potential. In most experimental studies, the electrode pores show a polydispersse distribution, which makes the size-dependent effects on Ψ_0^* and W less transparent[33, 34]. However, recent progress in the synthesis of carbide-derived carbons (CDC) enables a more precise pore-size control for porous electrodes. We expect that the theoretical predictions may be confirmed with experiments using these new kinds of materials[35].

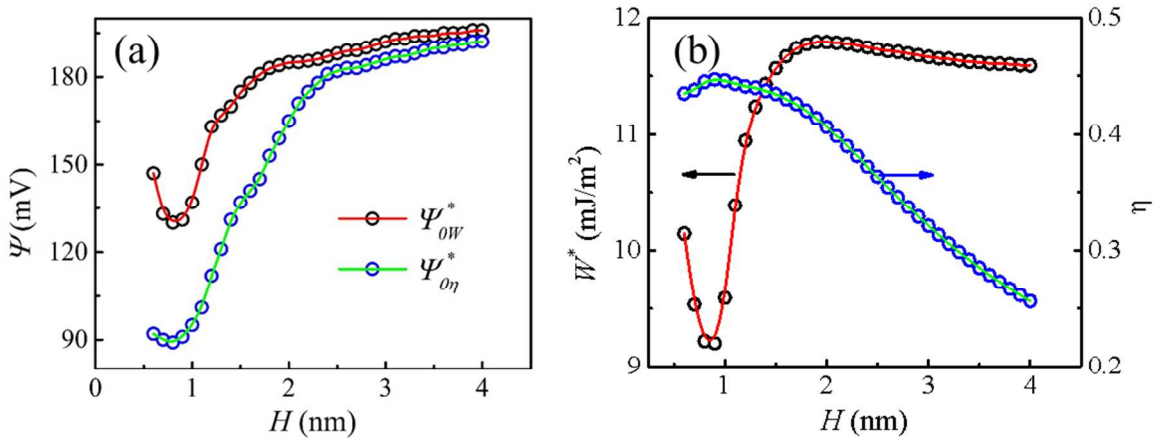

Figure 5 (a). Optimal charging potential as a function of the pore size based on the net extracted energy (Ψ_{0W}^*) and the thermodynamic efficiency ($\Psi_{0\eta}^*$); (b). Variations of the extracted energy W with the charging potential Ψ_{0W}^* and the thermodynamic efficiency with charging potential $\Psi_{0\eta}^*$ for electrodes of different pore sizes.

To explain the performance of the CDLE cycle in terms of the electrode pore size, we have also examined the density profiles of ions in different pores (shown in Figure S1). In

nanopores, the EDLs from the two sides of the slit pore interfere with each other, especially when the pore size is smaller than about 2 nm. The interference between the two opposing EDLs makes the ion concentration in the slit pore higher than that in the bulk[36-39]. The interference disappears for large pores, especially in the case for seawater where the Debye length is relatively small. From Figure S1d, we see that when the pore size is above 2nm, the ionic density profiles in the pore become almost invariant with the pore size. As a result, the extracted work reaches a plateau as the pore size is further increased (Fig. 5b). The interference effect also explains the behavior of CDLE cycle at ~1nm. Figure S2 shows the average relative density as a function of pore size in seawater and river water. Also shown here is the difference between the relative densities. We see that, in terms of the reduced densities, the difference between seawater and river water inside the porous electrode changes non-monotonically with the pore size, explaining the non-monotonic behavior of CDLE cycle near 1 nm.

Conclusions

We have studied the charging behavior of Capacitive Double Layer Expansion (CDLE) processes using a classical density functional theory (CDFT) that accounts for ion excluded volume effects and electrostatic correlations. We find that 1) for an electrode with a given pore size, there exists an optimal charging potential to maximize the net electrical energy output per cycle; 2) the optimal charging potential depends on the pore size, especially when it is smaller than 2 nm; and 3) the thermodynamic efficiency of the CDLE process also depends on the pore size and shows a maximum value when the pore size is about twice the ion diameter. These findings are significant from a practical perspective because by tuning the electrode pore size and operation conditions, the thermodynamic efficiency can be increased several fold without drastically compromising the work output. Such effects are not captured by conventional

methods for describing electrical double layers. The theoretical results on the pore size effects predicted in this work may be validated with experiments using novel porous electrode materials like the carbide-derived carbons (CDC).

ASSOCIATED CONTENT

Supporting Information. It provides expressions for the local excess chemical potentials due to ion size and charge correlations used in the DFT calculations. This material is available free of charge via the Internet.

AUTHOR INFORMATION

Corresponding Author

*E-mail: jwu@engr.ucr.edu (J.W.).

*E-mail: ludiannan@tsinghua.edu.cn (D.L.).

*E-mail: liuzheng@mail.tsinghua.edu.cn (Z.L.).

Notes

The authors declare no competing financial interest.

ACKNOWLEDGMENT

K.X. is grateful to the Chinese Scholarship Council for the visiting fellowship. This research is sponsored by the Fluid Interface Reactions, Structures, and Transport (FIRST) Center and the U.S. Department of Energy (DE-FG02-06ER46296). Additional support is provided by the National Natural Science foundation of China, No. 21276138, and Tsinghua University Foundation, No. 2013108930. The numerical calculations were performed at the National Energy Research Scientific Computing Center (NERSC).

REFERENCES

1. R. E. Pattle, *Nature*, 1954, 174, 660-660.

2. Z. Jia, B. Wang, S. Song and Y. Fan, *Renewable and Sustainable Energy Reviews*, 2014, 31, 91-100.
3. M. F. M. Bijmans, O. S. Burheim, M. Bryjak, A. Delgado, P. Hack, F. Mantegazza, S. Tenisson and H. V. M. Hamelers, *Enrgy Proced*, 2012, 20, 108-115.
4. D. Brogioli, R. Ziano, R. A. Rica, D. Salerno, O. Kozynchenko, H. V. M. Hamelers and F. Mantegazza, *Energ Environ Sci*, 2012, 5, 9870-9880.
5. D. Brogioli, *Phys Rev Lett*, 2009, 103.
6. B. B. Sales, M. Saakes, J. W. Post, C. J. N. Buisman, P. M. Biesheuvel and H. V. M. Hamelers, *Environ Sci Technol*, 2010, 44, 5661-5665.
7. F. La Mantia, M. Pasta, H. D. Deshazer, B. E. Logan and Y. Cui, *Nano Lett*, 2011, 11, 1810-1813.
8. Y. Oren, *Desalination*, 2008, 228, 10-29.
9. J. B. Lee, K. K. Park, H. M. Eum and C. W. Lee, *Desalination*, 2006, 196, 125-134.
10. M. Pasta, C. D. Wessells, Y. Cui and F. La Mantia, *Nano Lett*, 2012, 12, 839-843.
11. R. A. Rica, R. Ziano, D. Salerno, F. Mantegazza, R. van Roij and D. Brogioli, *Entropy*, 2013, 15, 1388-1407.
12. M. Janssen, A. Hartel and R. van Roij, *Phys Rev Lett*, 2014, 113, Artn 268501.
13. M. V. Fedorov and A. A. Kornyshev, *Chem Rev*, 2014, 114, 2978-3036.
14. S. Kondrat, C. R. Perez, V. Presser, Y. Gogotsi and A. A. Kornyshev, *Energ Environ Sci*, 2012, 5, 6474-6479.
15. E. Frackowiak, *Phys Chem Chem Phys*, 2007, 9, 1774-1785.
16. J. Chmiola, G. Yushin, Y. Gogotsi, C. Portet, P. Simon and P. L. Taberna, *Science*, 2006, 313, 1760-1763.
17. E. Raymundo-Pinero, K. Kierzek, J. Machnikowski and F. Beguin, *Carbon*, 2006, 44, 2498-2507.
18. C. Largeot, C. Portet, J. Chmiola, P. L. Taberna, Y. Gogotsi and P. Simon, *J Am Chem Soc*, 2008, 130, 2730-+.
19. R. B. Schoch, J. Y. Han and P. Renaud, *Rev Mod Phys*, 2008, 80, 839-883.
20. L. Bocquet and E. Charlaix, *Chem Soc Rev*, 2010, 39, 1073-1095.
21. D. Brogioli, R. Ziano, R. A. Rica, D. Salerno and F. Mantegazza, *J Colloid Interf Sci*, 2013, 407, 457-466.
22. A. Hartel, M. Janssen, S. Samin and R. van Roij, *J Phys-Condens Mat*, 2015, 27, Artn 194129.
23. N. Boon and R. van Roij, *Mol Phys*, 2011, 109, 1229-1241.
24. A. Hartel, M. Janssen, S. Samin and R. van Roij, *J Phys-Condens Mat*, 2015, 27.
25. Z. Li and J. Wu, *The Journal of Physical Chemistry B*, 2006, 110, 7473-7484.
26. Z. Li and J. Wu, *Physical Review E*, 2004, 70, 031109.
27. J. Wu and Z. Li, *Annual Review of Physical Chemistry*, 2007, 58, 85-112.
28. R. Zhao, P. M. Biesheuvel, H. Miedema, H. Bruning and A. van der Wal, *J Phys Chem Lett*, 2010, 1, 205-210.
29. in *Fundamentals of Interface and Colloid Science*, eds. A. d. K. Lyklema and M. A. C. Stuart, Academic Press, 1995, vol. Volume 2, pp. 1-232.
30. D. Brogioli, R. Zhao and P. M. Biesheuvel, *Energ Environ Sci*, 2011, 4, 772-777.
31. M. Marino, L. Misuri, M. L. Jimenez, S. Ahualli, O. Kozynchenko, S. Tennison, M. Bryjak and D. Brogioli, *J Colloid Interf Sci*, 2014, 436, 146-153.

32. M. L. Jimenez, M. M. Fernandez, S. Ahualli, G. Iglesias and A. V. Delgado, *J Colloid Interf Sci*, 2013, 402, 340-349.
33. T. A. Centeno, O. Sereda and F. Stoeckli, *Phys Chem Chem Phys*, 2011, 13, 12403-12406.
34. D.-e. Jiang, Z. Jin and J. Wu, *Nano Lett*, 2011, 11, 5373-5377.
35. V. Presser, M. Heon and Y. Gogotsi, *Advanced Functional Materials*, 2011, 21, 810-833.
36. D. E. Jiang, Z. H. Jin, D. Henderson and J. Z. Wu, *J Phys Chem Lett*, 2012, 3, 1727-1731.
37. D. E. Jiang and J. Z. Wu, *J Phys Chem Lett*, 2013, 4, 1260-1267.
38. J. Chmiola, C. Largeot, P. L. Taberna, P. Simon and Y. Gogotsi, *Angew Chem Int Edit*, 2008, 47, 3392-3395.
39. P. Simon and Y. Gogotsi, *Philos T R Soc A*, 2010, 368, 3457-3467.

Table of Contents (TOC) Graphic